Radiative Rate Enhancements in Ensembles of Hybrid Metal-Semiconductor Nanostructures

Yikuan Wang, Tianyu Yang, Mark T. Tuominen, and Marc Achermann*

Physics Department, University of Massachusetts Amherst, Amherst, Massachusetts 01003, USA

(Received 4 November 2008; published 23 April 2009)

We report on radiative decay rate modifications of dipole emitters in the proximity of anisotropic metal nanostructures. Using time, angle, and polarization resolved photoluminescence spectroscopy, we show that resonant interactions between surface plasmons in gold nanodisks and excitons in semiconductor nanocrystals require both spectral and orientational overlap resulting in radiative rate enhancements with directional characteristics. Numerical simulations of emission decay dynamics based on local electric field enhancements are in excellent agreement with experimental results.

DOI: 10.1103/PhysRevLett.102.163001 PACS numbers: 33.70.Ca, 73.20.Mf, 78.47.Cd, 78.67.Bf

First suggested for radio frequencies, Purcell's discovery that the spontaneous decay rate of a transition can be modified by coupling it to a resonant system has found many implementations for enhancing transition rates at optical frequencies [1,2]. It has been shown that the transition rate depends on the local electromagnetic mode density and can be increased by a proximal resonant system. At optical frequencies, nanoscale metal structures exhibit strong resonances caused by collective oscillations of free electrons known as surface plasmons (SPs) [3]. The resonant coupling of an emitter to SPs has attracted much attention for its potential to increase emission efficiencies of light emitting devices [4] and the sensitivity of fluorescence based sensors [5]. SP-induced radiative rate enhancement is a resonant process that occurs in the near field, requiring spectrally overlapping emitter and SP energies and precise positioning of the emitter in the vicinity of the metal nanostructure [6–13]. In addition, the emission dipole moment has to be oriented such that the interaction with SPs is allowed by a nonzero matrix element. Hence, in an anisotropic metal nanostructure that exhibits angular and polarization dependent SP resonances, coupling between dipole emitters and SPs is expected to modify the emission direction and polarization [14–17] and to lead to an enhancement of the radiative decay rate that depends on the emitter-SP coupling angle.

In this Letter, we determine radiative decay rate enhancements in hybrid structures comprised of dipole emitters and anisotropic metal nanostructures. We demonstrate for the first time that the photoluminescence (PL) decay dynamics of optically excited semiconductor nanocrystals (NCs) that are deposited on a gold disk array is accelerated when detected at a wavelength, angle, and polarization that correspond to a maximum in extinction measurements. Since the extinction spectra are dominated by SP effects, the accelerated decay is attributed to NC-SP interactions and, more specifically, to an increased *radiative* rate caused by local field enhancements in the vicinity of the metal nanostructures. Numerical calculations of the microscopic electric field distribution allow us to model the modified emission dynamics for the two cases of radiative and nonradiative rate changes. Consistent with our assertion, we find excellent agreement between experimental and modeled PL decay dynamics when radiative effects are considered to be dominant.

To study radiative decay rate enhancements in plasmonic nanoresonators, we fabricated square arrays of gold nanodisks with nominal dimensions of 170 nm diameter, 300 nm center-to-center distance, and 70 nm height [Fig. 1(a)]. The disk arrays were produced by high-resolution electron beam lithography and subsequent metal evaporation on a 100 nm thick SiN membrane that was suspended on a silicon wafer [18]. We characterized the Au disk arrays with angle and polarization resolved transmission measurements using a tungsten halogen light source that was lightly focused onto the sample [Fig. 1(b)]. From the transmission spectra measured through the SiN membrane with and without disk array, $I(\theta, \lambda)$ and $I_0(\theta, \lambda)$, respectively, we calculate the extinction $Q = -\ln[I(\theta, \lambda)/I_0(\theta, \lambda)]$ that we show in Fig. 1 as a function of angle θ, wavelength λ, and for p and s polarizations.

The extinction maps feature SP resonances and diffraction phenomena [19]. The extinction maximum at $\sim$800 nm is independent of polarization, has little angle dispersion, and can be associated with the in-plane $SP^{\parallel}$ resonance. In contrast, the extinction resonance at $\sim$600 nm is only active for p-polarized light at off-normal angles and can be related to the out-of-plane $SP^{\perp}$ resonance of the Au nanodisks [Fig. 1(c)]. The spectral width of the $SP^{\perp}$ resonance is mainly limited by homogeneous broadening since the height variation across the sample area (0.2×0.2 mm^2) is very small, whereas the $SP^{\parallel}$ resonance is significantly broadened by inhomogeneities of the lateral disk shapes.

Here, we focus on the interaction between excited NCs and the $SP^{\perp}$ resonance of the gold array that is only active for p-polarized, off-normal incidence light. It allows us to test the hypothesis that emission rate enhancement depends on the orientation and polarization of the dipole emitter with respect to the SP resonance and that NC-SP interactions can result in directionally enhanced emission. Conceptually, the radiative decay rates of NCs with or

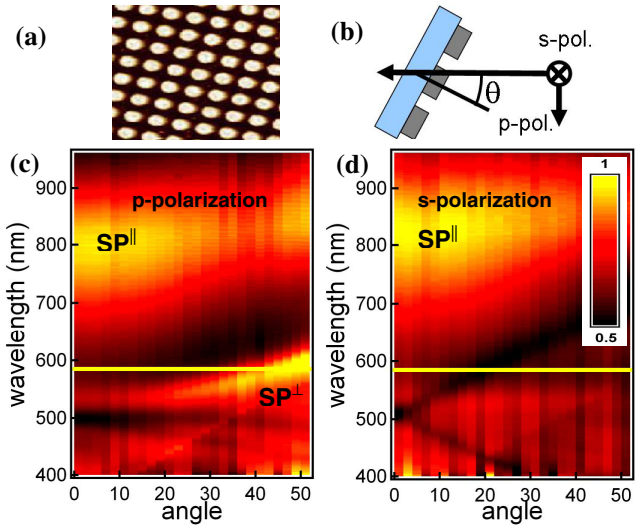

FIG. 1 (color online). (a) Atomic force microscope image of a square array of Au disks. (b) Definition of the angle and polarizations in the extinction setup. (c) and (d), p- and s-polarized extinction maps of the Au disk array as a function of θ and wavelength. Indicated are in-plan $SP^{\parallel}$ and out-of-plane $SP^{\perp}$ resonances and the PL wavelength of the NCs (yellow line).

without a metal nanostructure in their proximity, $\Gamma_{\mathrm{rad}}^{\mathrm{SP}}$ and Γ_{rad}, respectively, are related by the field enhancement factor F that is defined by the ratio of the projected local electric field onto the dipole direction with and without a metal nanostructure [6,8,20]:

$$\Gamma_{\mathrm{rad}}^{\mathrm{SP}} = |F|^2 \Gamma_{\mathrm{rad}}. \quad (1)$$

As dipole emitters we chose CdSe (ZnS) core (shell) NCs with an emission centered about 585 nm that overlaps with the $SP^{\perp}$ resonance (Fig. 1). We deposited NCs by spin coating onto the gold nanodisk arrays and obtained an approximate monolayer of NCs (determined by absorption measurements) with randomly oriented emission dipoles that cover the Au disks and the substrate between the disks. Using a NC monolayer ensures that all NCs have the same small separation from the surface of the Au disks or the substrate, which results in strong NC-SP near-field interactions and simplifies interpretation of the results and numerical modeling of the experiment. Extinction measurements after NC deposition revealed that the SP properties of the Au disk array are not significantly altered by the NC monolayer. Since a dipole emitter emits preferentially perpendicular to its dipole moment with a polarization parallel to the dipole moment, an angular and polarization sensitive detection scheme allows us to probe a subset of NCs with specific emission dipoles. Hence, depending on the emission wavelength, detection angle, and polarization, we can probe NCs that are in or out of resonance with SPs [14].

The schematic of our setup to measure SP-induced radiative rate modifications of dipole emitters in the proximity of metal nanostructures is shown in Fig. 2(a). We use a pulsed diode laser emitting ~50 ps pulses at 407 nm and 10 MHz repetition rate to excite the NCs at a fixed off-normal angle. At the excitation wavelength, all NCs in the monolayer can be excited independently of their crystalline orientation with respect to the excitation pulse direction and polarization, because the absorption of high-energy photons is caused by a dense manifold of electronic levels. The emission of the NCs, that is determined by the orientation of their two-dimensional emission dipoles and their local environment, is collected at variable angle and polarization [Fig. 2(a)]. The PL is then spectrally dispersed in a monochromator, detected at $\lambda = 585$ nm with a multichannel plate photomultiplier, and analyzed with a time-correlated single photon counting system with ~70 ps time resolution, yielding time, angle, and polarization resolved PL dynamics [21].

In Fig. 2 we show the time-resolved PL decay dynamics of the NCs on the Au disk array detected at different angles and PL polarizations. We find that for p-polarized PL, the decay dynamics at $\theta = 50°$ show a significant initial acceleration [Fig. 2(c)] that is absent at $\theta = 0°$ detection angle. In contrast, the s-polarized PL dynamics is essentially independent on the detection angle [Fig. 2(d)] and identical to the p-polarized PL at $\theta = 0°$. From extinction measurements we know that the $SP^{\perp}$ resonance is excited with p-polarized light at $\theta = 50°$ and $\lambda = 585$ nm. At this wavelength no SP resonance can be excited at normal incidence or at any angle with s-polarized light. Hence, there is a direct correlation between the extinction and time-resolved PL measurements and we conclude that the accelerated PL dynamics can be assigned to the interaction

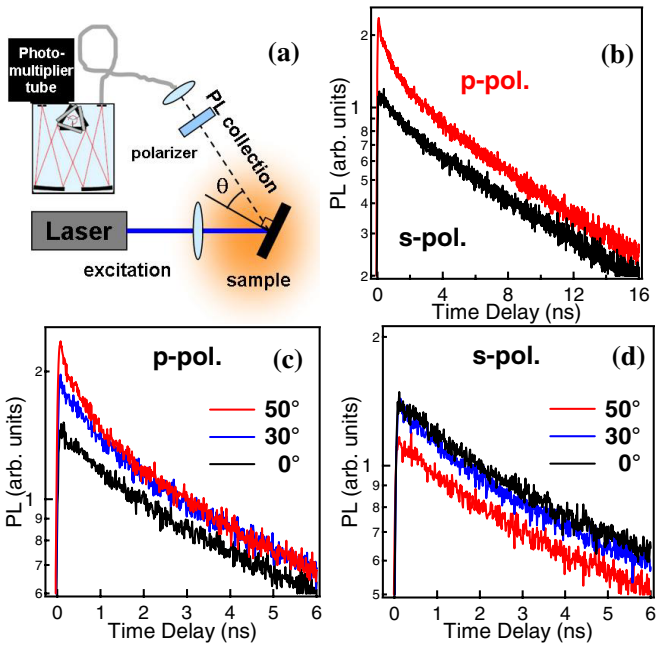

FIG. 2 (color online). (a) Schematic of the angle and polarization resolved PL dynamics setup. (b) p- and s-polarized PL decay dynamics collected at 50°. (c) and (d), p- and s-polarized PL dynamics obtained at 0°, 30°, and 50° collection angles.

between the NC dipole emitters and the $SP^{\perp}$ resonance. Such interaction is only significant when the NC dipole moments can excite SP oscillations. As a result of reciprocity relations that were generalized for evanescent waves in Ref. [20], the coupled NC-SP system scatters strongly into the 50° direction with *p*-polarized light, commensurate with the direction and polarization of large extinction values associated with SP excitations. *s* polarized PL or PL detected at normal incidence originate from NC dipole moments that cannot couple to a SP resonance and, therefore, PL decay dynamics are not accelerated.

For a more quantitative analysis of our measurements, one has to understand the emission decay dynamics of the assembled NCs. In the absence of SP effects, NC emission dynamics are determined by radiative recombination, nonradiative charge trapping into surface states, and fluorescence resonant energy transfer (FRET) from small NCs to large NCs within the quasimonodisperse size distribution of typical NC ensembles. From reference PL decay measurements of NC monolayers that were deposited on glass slides, we conclude that the dominant decay channel is radiative, consistent with the high NC quantum yield. FRET is found to be a small effect because of the ~5 nm NC radius (including CdSe core, ZnS shell, and hexadecylamin ligands) that gives rise to FRET times in the nanosecond range [21]. For NCs that are placed in the vicinity of a metal structure, an additional decay channel has to be taken into account, namely, emission quenching caused by Ohmic losses in the metal [6–11,22]. This nonradiative decay process is strongly distance dependent and of moderate efficiency at the ~5 nm separation of the NC from the Au disk surface. Considering these effects, the PL decay dynamics detected at $\theta = 0°$ can be modeled by the sum of two exponential decays with decay rates $\Gamma_m = \Gamma_{m,\mathrm{nr}} + \Gamma_{\mathrm{rad}}$ and $\Gamma_{\mathrm{sub}} = \Gamma_{\mathrm{nr}} + \Gamma_{\mathrm{rad}}$ that describe the emission dynamics of NCs that are located on the Au disks, Γ_m, and on the substrate between the Au disks, Γ_{sub}. Here, Γ_{nr} and $\Gamma_{m,\mathrm{nr}}$ are the nonradiative decay rates that include charge trapping, FRET between NCs, and metal quenching in the case of $\Gamma_{m,\mathrm{nr}}$. From a fit with a double exponential function we obtain $\Gamma_m = 0.7\ \mathrm{ns}^{-1}$ and $\Gamma_{\mathrm{sub}} = 0.1\ \mathrm{ns}^{-1}$. At $\theta = 50°$ detection angle, the PL decay that originates from NCs on Au disks is accelerated because of the interaction with the $SP^{\perp}$ resonance. Hence, the fast decay rate Γ_m changes with detection angle and we determine a decay rate difference of $\Delta\Gamma_m \approx 0.8\ \mathrm{ns}^{-1}$ between Γ_m at 0° and 50° detection angles. From the definition of Γ_m given above, we know that $\Delta\Gamma_m$ is caused by a change of the radiative or the nonradiative rate. Let us assume here that $\Delta\Gamma_m$ is associated with a SP-induced change of the *radiative* rate and *not* related to SP-induced nonradiative energy dissipation. We will provide evidence for this assumption below. From $\Delta\Gamma_m$ we can calculate the radiative rate enhancement $\Gamma_{\mathrm{rad}}^{\mathrm{SP}}/\Gamma_{\mathrm{rad}} = \Delta\Gamma_m/\Gamma_{\mathrm{rad}} + 1 \approx 11$, in which $\Gamma_{\mathrm{rad}} = 0.08\ \mathrm{ns}^{-1}$ is the reference radiative decay rate of NCs on the SiN substrate that was determined from the decay dynamics at long time delays [23]. Following Eq. (1), such radiative rate enhancement is associated with a field enhancement of ~3.3. The resonant nature of the decay rate enhancement is also manifested in its spectral dependence. We find a reduced enhancement at larger and smaller wavelengths obtained from measurements of the spectral tails of the inhomogeneously broadened NC emission.

The above assertion of a radiative rate enhancement is supported by the following reasoning. The time-resolved PL amplitude of an emitter at zero time delay, PL_0, is proportional to the radiative decay rate for energy conservation reasons, $\mathrm{PL}_0 \propto \Gamma_{\mathrm{rad}}$. Therefore, an increase of the radiative rate results in an increase of PL_0. In contrast, PL_0 remains unchanged for modifications of nonradiative decay rates. When comparing the non-normalized data taken at 50° for *s* and *p* polarizations [Fig. 2(b)], we find that PL_0 is significantly larger for *p*-polarized than for *s*-polarized emission. The same measurements of NCs on a glass slide or an unpatterned Au film did not show any significant polarization variations in the zero time delay amplitude or the decay dynamics. Likewise, in Fig. 2(c) we clearly see that PL_0 depends on the detection angle and is larger at higher angles. Such a behavior cannot be explained by nonradiative effects but has to be attributed to radiative rate changes.

As we have shown so far, our experimental results can be explained by hypothesizing that the fast decaying contribution of the total PL decay dynamics originates from the coupled NC-SP system that is characterized by a specific radiative rate enhancement factor. This interpretation depicts the basic physical mechanism, but is too simplified because the spatial distribution of the SP mode is not homogeneous on the disk surface [24]. One has to consider the local electric fields on a microscopic level in order to determine the NC-SP interactions. We used finite-difference time-domain (FDTD) numerical methods to calculate the normalized electric field distribution that is identical to the field enhancement factor *F*. In Figs. 3(a) and 3(b) we show *F* for *p*-polarized light at 50° incidence angle and at the $SP^{\perp}$ resonance wavelength that we obtained from the calculated extinction spectrum [Fig. 3(c)] [25]. The field enhancement is most pronounced on the top surface of the Au disks, confirming our assignment of the measured 585 nm extinction peak to the $SP^{\perp}$ resonance. The calculated field enhancement $F(x, y)$ allows us to determine the radiative decay rate using Eq. (1) based on the generalized reciprocity between absorption and emission of homogenous and evanescent waves and their angular components in the far and near field of local scatterers [20]. First, we assume that the NC-SP interaction is of purely radiative nature and simulate the PL decay dynamics, $\mathrm{PL}^{\mathrm{FDTD}}$, of NCs that are randomly distributed on the Au disk array:

$$\mathrm{PL}_{\mathrm{rad}}^{\mathrm{FDTD}}(t) \propto \int F^2(x, y)\Gamma_{\mathrm{rad}} e^{-F^2(x,y)\Gamma_{\mathrm{rad}} t}\, \partial x \partial y, \qquad (2)$$

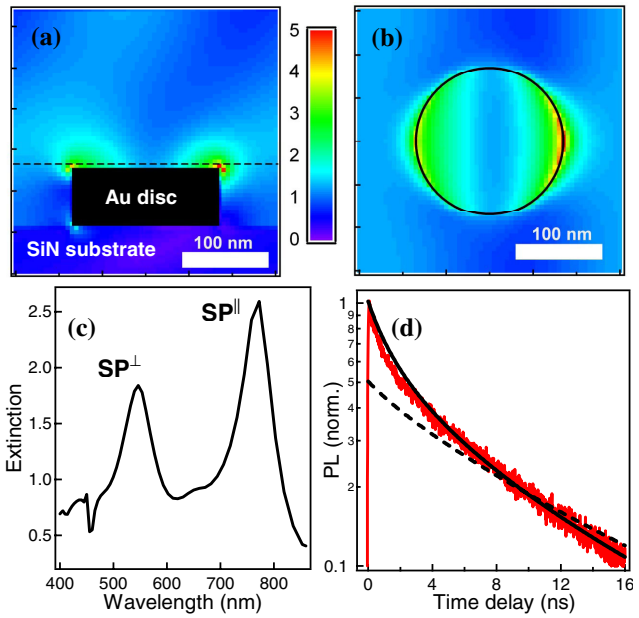

FIG. 3 (color online). FDTD calculations based on a p-polarized plane wave that is incident at 50° with a wavelength that corresponds to the $SP^{\perp}$ resonance at 50°: (a) Cross section of the field enhancement around an Au disk that is part of a square array. (b) Top view of the field enhancement at the z position shown in (a). The Au disk is indicated as a circle. (c) Calculated extinction at 50° [25]. (d) Measured (red line) and modeled PL dynamics based on SP-induced radiative (solid black line) and nonradiative (dashed black line) rate change.

in which the integration is performed over one unit cell of the disk array pattern at a constant height of 5 nm above the surface of the Au disk or the substrate. We considered the side walls of the Au disks to be NC free. As shown in Fig. 3(d), our calculations produce accelerated PL dynamics at short time delays that are caused by the SP-induced field enhancement on top of the Au disk. At longer time delays, PL dynamics approach the slower decay dynamic of NCs on the SiN substrate. Our calculated PL dynamics match very well with the experimental data supporting our interpretation that accelerated PL dynamics are caused by an SP-induced increase of the *radiative* rate. Moreover, the correspondence between calculated and measured dynamics illustrates the reciprocity between radiative rate enhancement and absorption and the consistency between the microscopic analysis in this section and the macroscopic interpretation of the previous paragraph. To demonstrate the effect of a possible nonradiative NC-SP interaction, we used the same spatial distribution of decay rates as in Eq. (2) but without the enhancement factor in the integration: $\mathrm{PL}_{\mathrm{nr}}^{\mathrm{FDTD}}(t) = \int e^{-F^2(x,y)\Gamma_{\mathrm{rad}}t}\partial x\partial y$. Figure 3(d) clearly shows that such a nonradiative interaction does not lead to a significant modification of the PL decay that remains dominated by the radiative PL dynamics of NCs on the substrate. This is in contrast to our measurements and we conclude that nonradiative NC-SP interactions cannot hold as an explanation for our experimental data.

In conclusion, we have measured the enhancement of radiative decay rates of emitters that interact with local SPs in anisotropic metal nanostructures. Our findings are derived from far-field PL decay and extinction measurements and are consistent with microscopic modeling of the near-field NC-SP interaction using the reciprocity theorem. Our results contribute to the fundamental understanding and modeling of optical interactions between emitters and SPs and facilitate the design and development of devices with engineered emission properties such as enhanced directional emission for lighting, optical sensing, and microscopy applications.

We would like to acknowledge the constructive comments of the reviewers and financial support from DARPA, Draper Labs, and NSF (Grant No. 0531171).

*achermann@physics.umass.edu

[1] E. M. Purcell, Phys. Rev. **69**, 681 (1946).
[2] D. Englund *et al.*, Phys. Rev. Lett. **95**, 013904 (2005).
[3] U. Kreibig and M. Vollmer, *Optical Properties of Metal Clusters* (Springer, Berlin, 1995).
[4] K. Okamoto *et al.*, Nature Mater. **3**, 601 (2004).
[5] F. Yu *et al.*, J. Am. Chem. Soc. **126**, 8902 (2004).
[6] K. T. Shimizu *et al.*, Phys. Rev. Lett. **89**, 117401 (2002).
[7] R. X. Bian, R. C. Dunn, and X. S. Xie, Phys. Rev. Lett. **75**, 4772 (1995).
[8] J. N. Farahani *et al.*, Phys. Rev. Lett. **95**, 017402 (2005).
[9] P. Anger, P. Bharadwaj, and L. Novotny, Phys. Rev. Lett. **96**, 113002 (2006).
[10] T. Soller *et al.*, Nano Lett. **7**, 1941 (2007).
[11] J. Seelig *et al.*, Nano Lett. **7**, 685 (2007).
[12] S. Kuhn *et al.*, Phys. Rev. Lett. **97**, 017402 (2006).
[13] O. L. Muskens *et al.*, Nano Lett. **7**, 2871 (2007).
[14] H. Mertens *et al.*, Nano Lett. **6**, 2622 (2006).
[15] T. H. Taminiau *et al.*, Nat. Photon. **2**, 234 (2008).
[16] K. Aslan, S. N. Malyn, and C. D. Geddes, Chem. Phys. Lett. **453**, 222 (2008).
[17] T. H. Taminiau, F. D. Stefani, and N. F. van Hulst, New J. Phys. **10**, 105005 (2008).
[18] Q. J. Xiao *et al.*, J. Appl. Phys. **103**, 07C521 (2008).
[19] T. A. Kelf *et al.*, Phys. Rev. Lett. **95**, 116802 (2005).
[20] R. Carminati, M. Neito-Vesperinas, and J. J. Greffet, J. Opt. Soc. Am. A **15**, 706 (1998).
[21] M. Achermann *et al.*, J. Phys. Chem. B **107**, 13 782 (2003).
[22] R. R. Chance, A. Prock, and R. Silbey, J. Chem. Phys. **60**, 2744 (1974).
[23] S. A. Crooker *et al.*, Appl. Phys. Lett. **82**, 2793 (2003).
[24] M. Achermann *et al.*, Opt. Lett. **32**, 2254 (2007).
[25] Though very similar, calculated and measured extinction spectra differ because of small differences in simulated and actual sample geometry and material parameters.